Arch Appl Mech (2011) 81:1555–1572
DOI 10.1007/s00419-010-0501-0

ORIGINAL

M. Bodaghi · A. R. Saidi

Thermoelastic buckling behavior of thick functionally graded rectangular plates

Received: 8 August 2010 / Accepted: 16 December 2010 / Published online: 7 January 2011

Abstract Thermoelastic buckling behavior of thick rectangular plate made of functionally graded materials is investigated in this article. The material properties of the plate are assumed to vary continuously through the thickness of the plate according to a power-law distribution. Three types of thermal loading as uniform temperature raise, nonlinear and linear temperature distribution through the thickness of plate are considered. The coupled governing stability equations are derived based on the Reddy's higher-order shear deformation plate theory using the energy method. The resulted stability equations are decoupled and solved analytically for the functionally graded rectangular plates with two opposite edges simply supported subjected to different types of thermal loading. A comparison of the present results with those available in the literature is carried out to establish the accuracy of the presented analytical method. The influences of power of functionally graded material, plate thickness, aspect ratio, thermal loading conditions and boundary conditions on the critical buckling temperature of aluminum/alumina functionally graded rectangular plates are investigated and discussed in detail. The critical buckling temperatures of thick functionally graded rectangular plates with various boundary conditions are reported for the first time and can be served as benchmark results for researchers to validate their numerical and analytical methods in the future.

Keywords Thermoelastic buckling · Functionally graded · Thick rectangular plate · Higher-order shear deformation theory · Analytical solution

List of symbols	
a, b	Length and width of plate, respectively
h	Plate thickness
x, y, z	Rectangular Cartesian coordinates
$P(z)$, P_c, P_m	Material properties of the functionally graded material (FGM), ceramic and metal
$E(z)$, E_c, E_m	Young's modulus of the FGM, ceramic and metal
$K(z)$, K_c, K_m	Coefficient of thermal conductivity of the FGM, ceramic and metal
$\alpha(z)$, α_c, α_m	Coefficient of thermal expansion of the FGM, ceramic and metal

M. Bodaghi · A. R. Saidi(✉)
Department of Mechanical Engineering, Shahid Bahonar University of Kerman, Kerman, Iran
E-mail: saidi@mail.uk.ac.ir
Tel.: +98-341-2111763
Fax: +98-341-2120964

n	Power of FGM
ν	Poisson's ratio
U_1, U_2, U_3	Components of displacement field
u, v, w	Displacements of mid-plane of the plate in the x, y and z directions, respectively
ψ_x, ψ_y	Rotation functions
$\varepsilon_{xx}, \varepsilon_{yy}$	Normal strains
$\gamma_{xy}, \gamma_{xz}, \gamma_{yz}$	Shear strains
σ_{xx}, σ_{yy}	Normal stresses
$\sigma_{xy}, \sigma_{xz}, \sigma_{yz}$	Shear stresses
Q_{11}, Q_{22}, Q_{12}	Elements of the reduced stiffness matrix
N_i, M_i, P_i, Q_j, R_j	Stress resultants
N^T, M^T, P^T	Thermal stress resultants
$T(x, y, z)$	Temperature distribution
T_c, T_m	Temperatures of full-ceramic and full-metallic surfaces of the plate
$A_{ij}, B_{ij}, C_{ij}, D_{ij}, F_{ij}, H_{ij}$	Plate stiffness coefficients
$u^0, v^0, w^0, \psi_x^0, \psi_y^0$	Displacement components related to equilibrium state
$u^1, v^1, w^1, \psi_x^1, \psi_y^1$	Incremental displacement components
$N_i^0, M_i^0, P_i^0, Q_j^0, R_j^0$	Stress resultants related to equilibrium state
$N_i^1, M_i^1, P_i^1, Q_j^1, R_j^1$	Incremental stress resultants
$B_1, B_2, \hat{B}, C_1, C_2, \hat{C}, \overline{C}, H_1, \hat{H}, A_2, \hat{A}, \hat{F}$	Constant material coefficients
$\overline{D}$	Equivalent flexural rigidity of the FG plate
φ_4	Boundary layer function
m	Number of half-waves in the x direction

1 Introduction

In recent years, a new class of composite materials known as functionally graded materials (FGMs) has gained considerable attention in engineering community, especially in high temperature applications such as nuclear reactors, aerospace and power generation industries. The functionally graded materials are microscopically heterogeneous materials in which the mechanical properties vary smoothly and continuously along certain dimension (usually in the thickness direction). This is achieved by gradually changing the volume fraction of the constituent materials. One of the main advantages of FGMs is that they mitigate cracks and remove the large interlaminar stresses at intersections between interfaces, which usually occur in the conventional laminated composite materials because of their abrupt variations in material compositions and properties. FGMs are typically made from a mixture of ceramic and metal in which the ceramic component provides high temperature resistance due to its low thermal conductivity, while the ductile metal component prevents fracture due to its greater toughness.

The functionally graded (FG) plates are commonly used in thermal environments; they can buckle under thermal and mechanical loads. Thus, the buckling analysis of such plates is essential to ensure an efficient and reliable design. The classical plate theory (CPT) is usually used to carry out stability analysis of thin FG plates [1]. This theory ignores the transverse shear deformation and assumes that the normal to the middle plane before deformation remains straight and normal to the middle surface after deformation. As a result, the classical plate theory overestimates the buckling load except for truly thin plates. The first-order shear deformation theory (FSDT), including the effects of transverse shear deformation, was employed by some researches to analyze buckling behavior of moderately thick FG plates [2,3]. The FSDT assumes a constant value of transverse shear strain through the thickness of the plate and requires shear correction factor to correct for the discrepancy between the actual transverse shear strain and the constant one. The shear correction factor, which is crucial to an accurate analysis, depends on geometric parameters, loadings, material and boundary conditions of the plate. Also in the FSDT, the cross-sectional warping is neglected as it is assumed that the plane sections remain plane. According to the viewpoint of some research groups, the first-order shear

deformation theory is not a proper model for analyzing thick plate structures [4–9]. To overcome the drawbacks of these theories (i.e., CPT and FSDT), various higher-order plate theories have been proposed by assuming higher-order displacement fields. Among these theories, the higher-order shear deformation theory (HSDT) of Reddy [4] has been extensively used for analysis of thick plates. The HSDT assumes third-order polynomials in the expansion of the displacement components through the thickness and accommodates a parabolic variation of the transverse shear strains and stresses through the thickness and the vanishing of transverse shear stresses on the top and bottom surfaces of the plate. Unlike the FSDT, the HSDT requires no shear correction factor and also the cross-sections of plate are allowed to warp.

Since the functionally graded plates do not have symmetry about the middle plane of the plate, their bending and stretching equations based on the higher-order shear deformation theory are highly coupled so that acquiring of an analytical solution becomes more complicated. Therefore, the analytical solutions for analyzing FG plate structures based on HSDT were limited to some simple cases like axisymmetric circular or simply supported rectangular plates due to the mathematical and computational complexities. Reddy [5] developed Navier solutions and finite element models for bending analysis of simply supported functionally graded rectangular plates based on the third-order shear deformation theory. Javaheri and Eslami [6] studied thermal buckling of simply supported FG plates subjected to various types of thermal loadings based on the higher-order shear deformation theory. They presented the buckling temperatures in closed-form solutions using Navier's method. Ma and Wang [7] employed the third-order shear deformation plate theory to solve the axisymmetric bending and buckling problems of functionally graded circular plates. They derived the relationships between the solutions of axisymmetric bending and buckling of FG plates based on the HSDT, and the solutions of the homogeneous plates obtained through the CPT. For special case of axisymmetric solid circular plate, buckling analysis of thick FG circular plates under uniform radial compression and thermal loading with clamped boundary conditions at circular edge was investigated by Najafizadeh and Heydari [8,9]. They presented closed-form solutions for the critical buckling load and temperature based on the HSDT. A finite element formulation for thermoelastic analysis of functionally graded plates and shells was developed by Naghdabadi and Hosseini Kordkheili [10]. Samsam Shariat and Eslami [11] presented the mechanical and thermal buckling analysis of thick functionally graded rectangular plates. They used the third-order shear deformation plate theory and Navier's method to obtain the closed-form solutions for the critical buckling load and temperature of a simply supported rectangular plate whose material properties vary linearly with respect to the thickness coordinate. Axisymmetric bending and buckling of functionally graded circular plates were investigated by Saidi et al. [12] based on the unconstrained third-order shear deformation plate theory. Recently, Bodaghi and Saidi [13] investigated mechanical buckling of thin functionally graded rectangular plates under nonlinearly varying in-plane loading resting on elastic foundation using classical plate theory.

Reformulation of coupled governing equations of plate by using the boundary layer function is an efficient method for solving plate problems based on shear deformation theories. There are some published articles in the literature that used this method for solving plate problems. Nosier and Reddy [14] showed that three bending equations of several refined linear theories of symmetric laminated plates, with transversely isotropic layers, can be uncoupled in two equations, one in terms of the transverse displacement and the other one in terms of the boundary layer function. Saidi and Jomehzadeh [15] presented an analytical solution for bending-stretching of FG rectangular plates with two opposite edges simply supported based on the first-order shear deformation theory using the boundary layer function. Mohammadi et al. [16] studied the buckling analysis of moderately thick FG rectangular plate based on the first-order plate theory.

To the best of authors' knowledge, there are no research works for thermal buckling analysis of functionally graded rectangular plates based on shear deformation plate theories in the open literature except for the simple special case of four edges simply supported plates. To investigate thermal buckling behavior of functionally graded rectangular plates in thermal environment with different boundary conditions, in this article a novel analytical method for thermal buckling analysis of thick functionally graded rectangular plates with two opposite edges simply supported and various boundary conditions along the other edges (Levy boundary conditions) has been developed. The derivation of the equations is based on the Reddy's higher-order shear deformation plate theory using the von Karman nonlinear kinematic relations. Introducing an analytical approach, the governing stability equations of functionally graded plates are decoupled and solved for a FG rectangular plate with two opposite edges simply supported under different thermal loads. By imposing different classical boundary conditions along two other opposite edges, the critical buckling temperatures are obtained for FG rectangular plates. The obtained results are compared with existing data in the literature. Moreover, the effect of power of FGM, thermal loading conditions, boundary conditions and geometric parameters of plate on the critical buckling temperature of Al/Al_2O_3 FG rectangular plate is comprehensively investigated.

2 Material properties of FG rectangular plate

Consider a functionally graded rectangular plate, which is made of ceramic and metal, and its properties vary through the thickness direction. The property variation is assumed to be in terms of a simple power-law distribution as [17]

$$P(z) = P_{cm}\left(\frac{1}{2} + \frac{z}{h}\right)^n + P_m \qquad P_{cm} = P_c - P_m \tag{1}$$

where the variable z is the thickness coordinate ($-h/2 \le z \le h/2$), h is the thickness of the plate and n denotes the power of FGM, which takes values greater than or equal to zero, also, P_m and P_c are the corresponding properties of the metal and ceramic, respectively. The variation of the composition of ceramic and metal is linear for $n = 1$. Also, the power of FGM equal to zero and infinity represents a fully ceramic and metallic plate, respectively. In this study, Eq. (1) will be used as a model for the coefficient of thermal conductivity K, coefficient of thermal expansion α and Young's modulus E of FG plates. The variation of Poisson's ratio ν is generally small, and it is assumed to be a constant [5–13].

3 Mathematical formulations

3.1 Equilibrium and stability equations based on the HSDT

Based on the higher-order shear deformation plate theory of Reddy, the displacement components of a material point within the plate domain in Cartesian coordinates system may be expressed as follows [4]

$$\begin{aligned} U_1(x, y, z) &= u(x, y) + z\psi_x(x, y) - \eta z^3[\psi_x(x, y) + w_{,x}] \\ U_2(x, y, z) &= v(x, y) + z\psi_y(x, y) - \eta z^3[\psi_y(x, y) + w_{,y}] \\ U_3(x, y, z) &= w(x, y) \end{aligned} \tag{2}$$

where u, v and w denote the displacements of a point on the mid-plane of the plate along x, y, and z coordinates, respectively, ψ_x and ψ_y are rotation functions of the middle surface and $\eta = \frac{4}{3h^2}$. Also, a comma denotes partial differentiation with respect to the Cartesian coordinates.

Upon substitution of Eq. (2) into the nonlinear strain–displacement relations in von Karman sense [18], the kinematic relations are obtained as follows

$$\begin{pmatrix} \varepsilon_{xx} \\ \varepsilon_{yy} \\ \gamma_{xy} \end{pmatrix} = \begin{pmatrix} \varepsilon_{xx}^{(0)} \\ \varepsilon_{yy}^{(0)} \\ \gamma_{xy}^{(0)} \end{pmatrix} + z\begin{pmatrix} \varepsilon_{xx}^{(1)} \\ \varepsilon_{yy}^{(1)} \\ \gamma_{xy}^{(1)} \end{pmatrix} + z^3\begin{pmatrix} \varepsilon_{xx}^{(3)} \\ \varepsilon_{yy}^{(3)} \\ \gamma_{xy}^{(3)} \end{pmatrix} \qquad \begin{pmatrix} \gamma_{xz} \\ \gamma_{yz} \end{pmatrix} = \begin{pmatrix} \gamma_{xz}^{(0)} \\ \gamma_{yz}^{(0)} \end{pmatrix} + z^2\begin{pmatrix} \gamma_{xz}^{(2)} \\ \gamma_{yz}^{(2)} \end{pmatrix} \tag{3}$$

where

$$\begin{pmatrix} \varepsilon_{xx}^{(0)} \\ \varepsilon_{yy}^{(0)} \\ \gamma_{xy}^{(0)} \end{pmatrix} = \begin{pmatrix} u_{,x} + (w_{,x})^2/2 \\ v_{,y} + (w_{,y})^2/2 \\ u_{,y} + v_{,x} + w_{,x}w_{,y} \end{pmatrix}; \quad \begin{pmatrix} \varepsilon_{xx}^{(1)} \\ \varepsilon_{yy}^{(1)} \\ \gamma_{xy}^{(1)} \end{pmatrix} = \begin{pmatrix} \psi_{x,x} \\ \psi_{y,y} \\ \psi_{x,y} + \psi_{y,x} \end{pmatrix}; \quad \begin{pmatrix} \varepsilon_{xx}^{(3)} \\ \varepsilon_{yy}^{(3)} \\ \gamma_{xy}^{(3)} \end{pmatrix} = -\eta\begin{pmatrix} \psi_{x,x} + w_{,xx} \\ \psi_{y,y} + w_{,yy} \\ \psi_{x,y} + \psi_{y,x} + 2w_{,xy} \end{pmatrix}$$
$$\begin{pmatrix} \gamma_{xz}^{(0)} \\ \gamma_{yz}^{(0)} \end{pmatrix} = \begin{pmatrix} \psi_x + w_{,x} \\ \psi_y + w_{,y} \end{pmatrix}; \quad \begin{pmatrix} \gamma_{xz}^{(2)} \\ \gamma_{yz}^{(2)} \end{pmatrix} = -\beta\begin{pmatrix} \psi_x + w_{,x} \\ \psi_y + w_{,y} \end{pmatrix}; \quad \beta = 3\eta = 4/h^2 \tag{4}$$

Based on relations (3) and using the principle of minimum total potential energy [19], the equilibrium equations are obtained as

$$\begin{aligned}
\delta u &: N_{xx,x} + N_{xy,y} = 0 \\
\delta v &: N_{xy,x} + N_{yy,y} = 0 \\
\delta \psi_x &: M_{xx,x} + M_{xy,y} - Q_x - \eta(P_{xx,x} + P_{xy,y}) + \beta R_x = 0 \\
\delta \psi_y &: M_{xy,x} + M_{yy,y} - Q_y - \eta(P_{xy,x} + P_{yy,y}) + \beta R_y = 0 \\
\delta w &: Q_{x,x} + Q_{y,y} + \eta(P_{xx,xx} + 2P_{xy,xy} + P_{yy,yy}) - \beta(R_{x,x} + R_{y,y}) \\
&\quad + N_{xx}w_{,xx} + 2N_{xy}w_{,xy} + N_{yy}w_{,yy} = 0
\end{aligned} \tag{5}$$

where δ represents the variational symbol; N_i, M_i, P_i, $(i = xx, yy, xy)$ are the resultant forces, moments, and higher-order moments, respectively, and Q_j, R_j, $(j = x, y)$ are, respectively, the shear forces and higher-order shear forces which are all defined by the following expressions

$$(N_i, M_i, P_i) = \int_{-h/2}^{h/2} (1, z, z^3)\sigma_i dz, \quad (i = xx, yy, xy) \tag{6a}$$

$$(Q_j, R_j) = \int_{-h/2}^{h/2} (1, z^2)\sigma_{jz} dz, \quad (j = x, y) \tag{6b}$$

The plane-stress reduced constitutive relations of the plate, taking into account the thermal effects are given by [20]

$$\begin{Bmatrix} \sigma_{xx} \\ \sigma_{yy} \\ \sigma_{xy} \\ \sigma_{xz} \\ \sigma_{yz} \end{Bmatrix} = \begin{bmatrix} Q_{11} & Q_{12} & 0 & 0 & 0 \\ Q_{12} & Q_{11} & 0 & 0 & 0 \\ 0 & 0 & Q_{22} & 0 & 0 \\ 0 & 0 & 0 & Q_{22} & 0 \\ 0 & 0 & 0 & 0 & Q_{22} \end{bmatrix} \left(\begin{Bmatrix} \varepsilon_{xx} \\ \varepsilon_{yy} \\ \gamma_{xy} \\ \gamma_{xz} \\ \gamma_{yz} \end{Bmatrix} - \begin{Bmatrix} 1 \\ 1 \\ 0 \\ 0 \\ 0 \end{Bmatrix} \alpha T \right) \tag{7}$$

where

$$Q_{11} = \frac{E}{(1-\nu^2)}; \quad Q_{12} = \nu Q_{11}; \quad Q_{22} = \frac{E}{2(1+\nu)} \tag{8}$$

where $T = T(x, y, z)$ is the temperature difference with respect to the reference temperature at which there are no thermal strains. Also, E and α are, respectively, the Young modulus and the coefficient of thermal expansion, which have been assumed to vary according to the power law Eq. (1).

Upon substitution of Eq. (3) into Eq. (7) and the subsequent results into Eq. (6), the stress resultants are obtained in the matrix form as

$$\begin{Bmatrix} N_{xx} \\ N_{yy} \\ N_{xy} \\ M_{xx} \\ M_{yy} \\ M_{xy} \\ P_{xx} \\ P_{yy} \\ P_{xy} \end{Bmatrix} = \begin{bmatrix} A_{11} & A_{12} & 0 & B_{11} & B_{12} & 0 & -\eta D_{11} & -\eta D_{12} & 0 \\ A_{12} & A_{11} & 0 & B_{12} & B_{11} & 0 & -\eta D_{12} & -\eta D_{11} & 0 \\ 0 & 0 & A_{22} & 0 & 0 & B_{22} & 0 & 0 & -\eta D_{22} \\ B_{11} & B_{12} & 0 & C_{11} & C_{12} & 0 & -\eta F_{11} & -\eta F_{12} & 0 \\ B_{12} & B_{11} & 0 & C_{12} & C_{11} & 0 & -\eta F_{12} & -\eta F_{11} & 0 \\ 0 & 0 & B_{22} & 0 & 0 & C_{22} & 0 & 0 & -\eta F_{22} \\ D_{11} & D_{12} & 0 & F_{11} & F_{12} & 0 & -\eta H_{11} & -\eta H_{12} & 0 \\ D_{12} & D_{11} & 0 & F_{12} & F_{11} & 0 & -\eta H_{12} & -\eta H_{11} & 0 \\ 0 & 0 & D_{22} & 0 & 0 & F_{22} & 0 & 0 & -\eta H_{22} \end{bmatrix} \begin{Bmatrix} u_{,x} + (w_{,x})^2/2 \\ v_{,y} + (w_{,y})^2/2 \\ u_{,y} + v_{,x} + w_{,x}w_{,y} \\ \psi_{x,x} \\ \psi_{y,y} \\ \psi_{x,y} + \psi_{y,x} \\ \psi_{x,x} + w_{,xx} \\ \psi_{y,y} + w_{,yy} \\ \psi_{x,y} + \psi_{y,x} + 2w_{,xy} \end{Bmatrix} - \begin{Bmatrix} N^T \\ N^T \\ 0 \\ M^T \\ M^T \\ 0 \\ P^T \\ P^T \\ 0 \end{Bmatrix}$$

$$\begin{Bmatrix} Q_x \\ Q_y \\ R_x \\ R_y \end{Bmatrix} = \begin{bmatrix} A_{22} - \beta C_{22} & 0 \\ 0 & A_{22} - \beta C_{22} \\ C_{22} - \beta F_{22} & 0 \\ 0 & C_{22} - \beta F_{22} \end{bmatrix} \begin{Bmatrix} \psi_x + w_{,x} \\ \psi_y + w_{,y} \end{Bmatrix} \tag{9}$$

where $(A_{ij},\ B_{ij},\ C_{ij},\ D_{ij},\ F_{ij},\ H_{ij})$ are the plate stiffness coefficients, and N^T, M^T and P^T are the thermal force, moment and higher-order moment resultants due to the applied temperature field on the plate. These parameters are defined by the following expressions

$$(A_{ij}, B_{ij}, C_{ij}, D_{ij}, F_{ij}, H_{ij}) = \int_{-h/2}^{h/2} (1, z, z^2, z^3, z^4, z^6) Q_{ij} dz, \quad i, j = 1, 2 \tag{10a}$$

$$(N^T, M^T, P^T) = \int_{-h/2}^{h/2} (1, z, z^3)(Q_{11} + Q_{12}) \alpha T dz \tag{10b}$$

Focusing on relations (8) and (10a), it can be concluded that

$$(A_{12}, B_{12}, C_{12}, D_{12}, F_{12}, H_{12}) = (A_{11}, B_{11}, C_{11}, D_{11}, F_{11}, H_{11}) - 2(A_{22}, B_{22}, C_{22}, D_{22}, F_{22}, H_{22}) \tag{11}$$

In order to derive the stability equations and study the thermal buckling behavior of the FG plate, the adjacent equilibrium criterion is used [18]. Assume that the equilibrium state of a plate under thermal loads is defined in terms of the displacement components u^0, v^0, w^0, ψ_x^0 and ψ_y^0. Consider an infinitesimally small increment from the stable configuration whose displacement components differ by u^1, v^1, w^1, ψ_x^1 and ψ_y^1 with respect to the equilibrium position. Thus, the total displacement and rotation functions of a neighboring configuration of the stable state can be expressed as follows

$$\begin{aligned} &u = u^0 + u^1; \quad v = v^0 + v^1; \quad w = w^0 + w^1 \\ &\psi_x = \psi_x^0 + \psi_x^1; \quad \psi_y = \psi_y^0 + \psi_y^1 \end{aligned} \tag{12}$$

Upon substituting the relations (12) into Eq. (9), the expressions for the stress resultants related to the equilibrium and neighboring states are obtained. Equivalently, the stress resultants can be expressed as

$$\begin{cases} N_i = N_i^0 + N_i^1; \quad M_i = M_i^0 + M_i^1; \quad P_i = P_i^0 + P_i^1, \quad i = xx, yy, xy \\ R_j = R_j^0 + R_j^1; \quad Q_j = Q_j^0 + Q_j^1, \quad j = x, y \end{cases} \tag{13}$$

where the terms with subscripts 0 are corresponding to the equilibrium state and the terms with subscripts 1 are linear parts of the stress resultants increments corresponding to the neighboring state.

It is assumed that the temperature variation occurs in the thickness direction only and the temperature field is assumed to be constant in the $x - y$ plane of the plate. In such a case, the stability equations may be obtained by substituting Eqs. (12) and (13) into Eq. (5). Upon substitution, the terms in the resulting equations with superscript 0 satisfy the equilibrium condition and therefore omitted from the equations. Also, the nonlinear terms with superscript 1 will be ignored because they are small compared to the linear terms [11]. The remaining terms form the stability equations of functionally graded rectangular plate as

$$\begin{aligned} N_{xx,x}^1 + N_{xy,y}^1 &= 0 \\ N_{xy,x}^1 + N_{yy,y}^1 &= 0 \\ M_{xx,x}^1 + M_{xy,y}^1 - Q_x^1 - \eta\left(P_{xx,x}^1 + P_{xy,y}^1\right) + \beta R_x^1 &= 0 \\ M_{xy,x}^1 + M_{yy,y}^1 - Q_y^1 - \eta\left(P_{xy,x}^1 + P_{yy,y}^1\right) + \beta R_y^1 &= 0 \\ Q_{x,x}^1 + Q_{y,y}^1 + \eta\left(P_{xx,xx}^1 + 2P_{xy,xy}^1 + P_{yy,yy}^1\right) - \beta\left(R_{x,x}^1 + R_{y,y}^1\right) + N_{xx}^0 w_{,xx}^1 + 2N_{xy}^0 w_{,xy}^1 + N_{yy}^0 w_{,yy}^1 &= 0 \end{aligned} \tag{14}$$

3.2 The governing stability equations and their decoupled form

Substituting the equivalent neighboring form of Eq. (9) into stability Eq. (14) leads to the following governing stability equations

$$A_{11}u^1_{,xx}+A_{12}v^1_{,yx}+B_{11}\psi^1_{x,xx}+B_{12}\psi^1_{y,yx}-\eta D_{11}\left(\psi^1_{x,x}+w^1_{,xx}\right)_{,x}-\eta D_{12}\left(\psi^1_{y,y}+w^1_{,yy}\right)_{,x}$$
$$+A_{22}\left(u^1_{,y}+v^1_{,x}\right)_{,y}+B_{22}\left(\psi^1_{x,y}+\psi^1_{y,x}\right)_{,y}-\eta D_{22}\left(\psi^1_{x,y}+\psi^1_{y,x}+2w^1_{,xy}\right)_{,y}=0 \tag{15a}$$

$$A_{11}v^1_{,yy}+A_{12}u^1_{,xy}+B_{11}\psi^1_{y,yy}+B_{12}\psi^1_{x,xy}-\eta D_{11}\left(\psi^1_{y,y}+w^1_{,yy}\right)_{,y}-\eta D_{12}\left(\psi^1_{x,x}+w^1_{,xx}\right)_{,y}$$
$$+A_{22}\left(u^1_{,y}+v^1_{,x}\right)_{,x}+B_{22}\left(\psi^1_{x,y}+\psi^1_{y,x}\right)_{,x}-\eta D_{22}\left(\psi^1_{x,y}+\psi^1_{y,x}+2w^1_{,xy}\right)_{,x}=0 \tag{15b}$$

$$\left(B_{11}-\eta D_{11}\right)u^1_{,xx}+\left(B_{12}-\eta D_{12}\right)v^1_{,yx}+\left(C_{11}-\eta F_{11}\right)\psi^1_{x,xx}+\left(C_{12}-\eta F_{12}\right)\psi^1_{y,yx}$$
$$-\eta\left(F_{11}-\eta H_{11}\right)\left(\psi^1_{x,x}+w^1_{,xx}\right)_{,x}-\eta\left(F_{12}-\eta H_{12}\right)\left(\psi^1_{y,y}+w^1_{,yy}\right)_{,x}+\left(B_{22}-\eta D_{22}\right)\left(u^1_{,y}+v^1_{,x}\right)_{,y}$$
$$+\left(C_{22}-\eta F_{22}\right)\left(\psi^1_{x,y}+\psi^1_{y,x}\right)_{,y}-\eta\left(F_{22}-\eta H_{22}\right)\left(\psi^1_{x,y}+\psi^1_{y,x}+2w^1_{,xy}\right)_{,y}$$
$$-\left(A_{22}-2\beta C_{22}+\beta^2F_{22}\right)\left(\psi^1_{x}+w^1_{,x}\right)=0 \tag{15c}$$

$$\left(B_{11}-\eta D_{11}\right)v^1_{,yy}+\left(B_{12}-\eta D_{12}\right)u^1_{,xy}+\left(C_{11}-\eta F_{11}\right)\psi^1_{y,yy}+\left(C_{12}-\eta F_{12}\right)\psi^1_{x,xy}$$
$$-\eta\left(F_{11}-\eta H_{11}\right)\left(\psi^1_{y,y}+w^1_{,yy}\right)_{,y}-\eta\left(F_{12}-\eta H_{12}\right)\left(\psi^1_{x,x}+w^1_{,xx}\right)_{,y}+\left(B_{22}-\eta D_{22}\right)\left(u^1_{,y}+v^1_{,x}\right)_{,x}$$
$$+\left(C_{22}-\eta F_{22}\right)\left(\psi^1_{x,y}+\psi^1_{y,x}\right)_{,x}-\eta\left(F_{22}-\eta H_{22}\right)\left(\psi^1_{x,y}+\psi^1_{y,x}+2w^1_{,xy}\right)_{,x}$$
$$-\left(A_{22}-2\beta C_{22}+\beta^2F_{22}\right)\left(\psi^1_{y}+w^1_{,y}\right)=0 \tag{15d}$$

$$\eta\left\{D_{11}\left(u^1_{,xxx}+v^1_{,yyy}\right)+D_{12}\left(u^1_{,xyy}+v^1_{,yxx}\right)+F_{11}\left(\psi^1_{x,xxx}+\psi^1_{y,yyy}\right)+F_{12}\left(\psi^1_{x,xyy}+\psi^1_{y,yxx}\right)\right.$$
$$-\eta H_{11}\left[\left(\psi^1_{x,x}+w^1_{,xx}\right)_{,xx}+\left(\psi^1_{y,y}+w^1_{,yy}\right)_{,yy}\right]-\eta H_{12}\left[\left(\psi^1_{y,y}+w^1_{,yy}\right)_{,xx}+\left(\psi^1_{x,x}+w^1_{,xx}\right)_{,yy}\right]$$
$$\left.+2D_{22}\left(u^1_{,y}+v^1_{,x}\right)_{,xy}+2F_{22}\left(\psi^1_{x,y}+\psi^1_{y,x}\right)_{,xy}-2\eta H_{22}\left(\psi^1_{x,y}+\psi^1_{y,x}+2w^1_{,xy}\right)_{,xy}\right\}$$
$$+\left(A_{22}-2\beta C_{22}+\beta^2F_{22}\right)\left[\left(\psi^1_{x}+w^1_{,x}\right)_{,x}+\left(\psi^1_{y}+w^1_{,y}\right)_{,y}\right]+N^0_{xx}w^1_{,xx}+2N^0_{xy}w^1_{,xy}+N^0_{yy}w^1_{,yy}=0 \tag{15e}$$

The above equations are five highly coupled partial differential equations in terms of neighboring displacement components.

In order to facilitate the solutions of these coupled equations, they will be reformulated to decoupled equations. To this end, four new analytical functions are introduced as follows

$$\begin{Bmatrix}\varphi_1\\ \varphi_2\\ \varphi_3\\ \varphi_4\end{Bmatrix}=\begin{Bmatrix}u^1_{,x}+v^1_{,y}\\ u^1_{,y}-v^1_{,x}\\ \psi^1_{x,x}+\psi^1_{y,y}\\ \psi^1_{x,y}-\psi^1_{y,x}\end{Bmatrix} \tag{16}$$

By using relation (11) and above analytical functions, the governing stability Eq. (15) abbreviate to simpler form as

$$A_{11}\varphi_{1,x} + A_{22}\varphi_{2,y} + B_1\varphi_{3,x} + B_2\varphi_{4,y} - \eta D_{11}\nabla^2 w^1_{,x} = 0 \tag{17a}$$

$$A_{11}\varphi_{1,y} - A_{22}\varphi_{2,x} + B_1\varphi_{3,y} - B_2\varphi_{4,x} - \eta D_{11}\nabla^2 w^1_{,y} = 0 \tag{17b}$$

$$B_1\varphi_{1,x} + B_2\varphi_{2,y} + C_1\varphi_{3,x} + C_2\varphi_{4,y} - A_2\left(\psi^1_x + w^1_{,y}\right) - H_1\nabla^2 w^1_{,x} = 0 \tag{17c}$$

$$B_1\varphi_{1,y} - B_2\varphi_{2,x} + C_1\varphi_{3,y} - C_2\varphi_{4,x} - A_2\left(\psi^1_y + w^1_{,y}\right) - H_1\nabla^2 w^1_{,y} = 0 \tag{17d}$$

$$\eta D_{11}\nabla^2\varphi_1 + H_1\nabla^2\varphi_3 - \eta^2 H_{11}\nabla^4 w^1 + A_3\left(\nabla^2 w^1 + \varphi_3\right) + N^0_{xx}w^1_{,xx} + 2N^0_{xy}w^1_{,xy} + N^0_{yy}w^1_{,yy} = 0 \tag{17e}$$

where ∇^2 is two-dimensional Laplacian operator and the constant coefficients in Eq. (17) are defined as

$$\begin{aligned} B_1 &= B_{11} - \eta D_{11}, \quad & C_1 &= C_{11} - 2\eta F_{11} + \eta^2 H_{11} \\ B_2 &= B_{22} - \eta D_{22}, \quad & C_2 &= C_{22} - 2\eta F_{22} + \eta^2 H_{22} \\ H_1 &= \eta F_{11} - \eta^2 H_{11}, \quad & A_2 &= A_{22} - 2\beta C_{22} + \beta^2 F_{22} \end{aligned} \tag{18}$$

Multiplying Eq. (17a), (17b) by B_1/A_{11} and considering $B_2 = B_1 A_{22}/A_{11}$ yields

$$B_1\varphi_{1,x} + B_2\varphi_{2,y} = -\frac{B_1^2}{A_{11}}\varphi_{3,x} - \frac{B_1 B_2}{A_{11}}\varphi_{4,y} + \frac{\eta D_{11} B_1}{A_{11}}\nabla^2 w^1_{,x} \tag{19a}$$

$$B_1\varphi_{1,y} - B_2\varphi_{2,x} = -\frac{B_1^2}{A_{11}}\varphi_{3,y} + \frac{B_1 B_2}{A_{11}}\varphi_{4,x} + \frac{\eta D_{11} B_1}{A_{11}}\nabla^2 w^1_{,y} \tag{19b}$$

Also, differentiating Eq. (19a), (19b) with respect to x and y, respectively, and adding the results, the following relation is found

$$\nabla^2\varphi_1 = -\frac{B_1}{A_{11}}\nabla^2\varphi_3 + \frac{\eta D_{11}}{A_{11}}\nabla^4 w^1 \tag{20}$$

Moreover, from subtraction of the differentiation of Eq. (19a) with respect to y and Eq. (19b) with respect to x, it is concluded that

$$\nabla^2\varphi_2 = -\frac{B_1}{A_{11}}\nabla^2\varphi_4 \tag{21}$$

By using Eqs. (19) and (20), the last three equation of (17) can be rewritten as

$$\hat{C}\varphi_{3,x} + \hat{B}\varphi_{4,y} - \hat{A}\left(\psi^1_x + w^1_{,x}\right) - \hat{H}\nabla^2 w^1_{,x} = 0 \tag{22a}$$

$$\hat{C}\varphi_{3,y} - \hat{B}\varphi_{4,x} - \hat{A}\left(\psi^1_y + w^1_{,y}\right) - \hat{H}\nabla^2 w^1_{,y} = 0 \tag{22b}$$

$$\hat{H}\nabla^2\varphi_3 - \hat{F}\nabla^4 w^1 + \hat{A}\left(\nabla^2 w^1 + \varphi_3\right) + N^0_{xx}w^1_{,xx} + 2N^0_{xy}w^1_{,xy} + N^0_{yy}w^1_{,yy} = 0 \tag{22c}$$

where

$$\begin{aligned} \hat{C} &= C_1 - \frac{B_1^2}{A_{11}}, \quad \hat{B} = C_2 - \frac{B_1 B_2}{A_{11}}, \quad \hat{A} = A_2 \\ \hat{H} &= H_1 - \frac{\eta D_{11} B_1}{A_{11}}, \quad \hat{F} = \eta^2\left(H_{11} - \frac{D_{11}^2}{A_{11|}}\right) \end{aligned} \tag{23}$$

It can be seen that the in-plane displacements (u and v) do not exist in Eq. (22), and these equations are three partial differential equation in terms of the rotation functions (ψ_x and ψ_y) and the transverse displacement (w) only. In other words, Eq. (22) are the bending equations that are decoupled from the stretching equations.

Furthermore, using some algebraic calculations, three extensively coupled Eq. (22) can be converted into two independent equations as

$$\hat{B}\nabla^2\varphi_4 - \hat{A}\varphi_4 = 0 \tag{24a}$$

$$\overline{C}\nabla^6 w^1 - \overline{D}\nabla^4 w^1 = \frac{\hat{C}}{\hat{A}}\nabla^2\left(N^0_{xx}w^1_{,xx} + 2N^0_{xy}w^1_{,xy} + N^0_{yy}w^1_{,yy}\right) - \left(N^0_{xx}w^1_{,xx} + 2N^0_{xy}w^1_{,xy} + N^0_{yy}w^1_{,yy}\right) \tag{24b}$$

where the parameters $\overline{C}$, $\overline{D}$ are defined as

$$\overline{C} = \frac{\hat{F}\hat{C} - \hat{H}^2}{\hat{A}}, \quad \overline{D} = C_{11} - \frac{B^2_{11}}{A_{11}} \tag{25}$$

Equation (24a) is known as the edge-zone (or boundary layer) equation of the plate, and the function φ_4 is referred to the boundary layer function [14]. Also, Eq. (24b) is called the interior equation of the plate. These equations are similar to the equations for isotropic homogenous plates, reported previously by Nosier and Reddy [14]. But the definitions of parameters $\overline{C}$, $\overline{D}$, $\hat{C}$, $\hat{B}$ and $\hat{A}$ appeared in Eqs. (25) and (23) are different. This is due to the fact that the material properties of functionally graded plates vary through the thickness direction according to a power-law distribution, and, consequently, the plate stiffness coefficients from Eq. (10a) are differently obtained. This similarity in the stability equations configuration shows that the functionally graded plates behave like isotropic homogeneous plates [21]. For a homogeneous fully ceramic plate ($n = 0$), the parameters $\overline{C}$, $\overline{D}$, $\hat{C}$, $\hat{B}$ and $\hat{A}$ are simplified as $\frac{E_c h^5}{5040(1-\nu^2)(1-\nu)}$, $\frac{E_c h^3}{12(1-\nu^2)}$, $\frac{17E_c h^3}{315(1-\nu^2)}$, $\frac{E_c h^3}{630(1+\nu)}$ and $\frac{4E_c h}{15(1+\nu)}$, respectively. It should be mentioned that the parameter $\overline{D}$ denotes the equivalent flexural rigidity of the functionally graded plate.

The rotation functions can be expressed in terms of transverse displacement and boundary layer function as

$$\psi^1_x = \left(\frac{\hat{C}\overline{C}}{\hat{A}(\hat{C}+\hat{H})}\nabla^4 w^1 - \frac{(\hat{C}+\hat{H})}{\hat{A}}\nabla^2 w^1 - w^1 - \frac{\hat{C}^2}{\hat{A}^2(\hat{C}+\hat{H})}\left(N^0_{xx}w^1_{,xx} + 2N^0_{xy}w^1_{,xy} + N^0_{yy}w^1_{,yy}\right)\right)_{,x} + \frac{\hat{B}}{\hat{A}}\varphi_{4,y} \tag{26a}$$

$$\psi^1_y = \left(\frac{\hat{C}\overline{C}}{\hat{A}(\hat{C}+\hat{H})}\nabla^4 w^1 - \frac{(\hat{C}+\hat{H})}{\hat{A}}\nabla^2 w^1 - w^1 - \frac{\hat{C}^2}{\hat{A}^2(\hat{C}+\hat{H})}\left(N^0_{xx}w^1_{,xx} + 2N^0_{xy}w^1_{,xy} + N^0_{yy}w^1_{,yy}\right)\right)_{,y} - \frac{\hat{B}}{\hat{A}}\varphi_{4,x} \tag{26b}$$

Details of deriving Eqs. (24) and (26) are given in Appendix A.

Considering the definition of functions $\varphi_i (i = 1, 2, 3, 4)$ in relations (16), it is easy to show that the Eqs. (20) and (21) can be satisfied by assuming the in-plane displacements as follows

$$\begin{aligned} u^1 &= -\frac{B_{11}}{A_{11}}\psi^1_x + \frac{\eta D_{11}}{A_{11}}\left(\psi^1_x + w^1_{,x}\right) \\ v^1 &= -\frac{B_{11}}{A_{11}}\psi^1_y + \frac{\eta D_{11}}{A_{11}}\left(\psi^1_y + w^1_{,y}\right) \end{aligned} \tag{27}$$

It can be readily shown that relations (27) satisfy not only Eqs. (20) and (21), but also the boundary conditions of the plate. Note that the parameters B_{ij} and D_{ij} are zero for homogeneous isotropic plates so in this case, the in-plane displacements are equal to zero as expected.

3.3 Thermal buckling analysis

Consider a rectangular plate with the length a and width b subjected to thermal loading. It is assumed that two opposite edges of the plate at $x = 0$ and $x = a$ are hard type simply supported with movable in-plane displacements. To find the critical buckling temperature, the prebuckling thermal forces should be found. Thus, solving the membrane form of the equilibrium equations and using the method developed by Meyers and Hyer

[22], the prebuckling force resultants of FG plate exposed to the nonuniform temperature distribution across the thickness are found to be [1,3,6,11]

$$N_{xx}^0 = -N^T, \quad N_{yy}^0 = -N^T, \quad N_{xy}^0 = 0. \tag{28}$$

Substituting relations (28) into Eq. (24b) yields

$$\overline{C}\nabla^6 w^1 - \left(\overline{D} - \frac{\hat{C}}{\hat{A}}N^T\right)\nabla^4 w^1 - N^T\nabla^2 w^1 = 0. \tag{29}$$

To analyze thermal buckling behavior of functionally graded rectangular plates, the decoupled stability Eqs. (29) and (24a) should be solved. Since the plate is simply supported (hard type) along two opposite edges in y direction, the following series solutions are chosen for the transverse displacement w^1 and the function φ_4

$$w^1(x, y) = \sum_{m=1}^{\infty} f(y)\sin(\lambda_m x) \tag{30a}$$

$$\varphi_4(x, y) = \sum_{m=1}^{\infty} g(y)\cos(\lambda_m x) \tag{30b}$$

where λ_m denotes $m\pi/a$ and m is the number of half-waves in the x direction. It can be seen that Eq. (30) exactly satisfy the hard simply supported boundary conditions at $x = 0$ and $x = a$ $\left(w^1 = \psi_y^1 = M_{xx}^1 = P_{xx}^1 = 0\right)$. Upon substitution of Eq. (30a) into Eq. (29) and simplifying the result, the following ordinary differential equation can be obtained

$$f^{(6)}(y) - \left(3\lambda_m^2 + V\right)f^{(4)}(y) + \left(3\lambda_m^4 + 2V\lambda_m^2 - S\right)f^{(2)}(y) - \lambda_m^2\left(\lambda_m^4 + \lambda_m^2 V - S\right)f(y) = 0 \tag{31}$$

where

$$V = \frac{\overline{D}}{\overline{C}} - \frac{\hat{C}N^T}{\hat{A}\overline{C}}; \quad S = \frac{N^T}{\overline{C}}. \tag{32}$$

By investigating, it is observed that the general solution of Eq. (31) depends on the sign of $V^2/4 + S$ (positive, zero or negative). Since the sign of $V^2/4 + S$ depends on the unknown buckling temperature, it is necessary to investigate all the possible cases. Three general cases can occur as follows:

Case 1 $V^2/4 + S > 0$

In this case, the general solution of Eq. (31) involves the hyperbolic functions with six unknown constants of integration as follows

$$\begin{aligned} f(y) = {} & c_1\cos\text{h}(\lambda_m y) + c_2\sin\text{h}(\lambda_m y) + c_3\cos\text{h}(\theta_1 y) + c_4\sin\text{h}(\theta_1 y) \\ & + c_5\cos\text{h}(\mu_1 y) + c_6\sin\text{h}(\mu_1 y) \end{aligned} \tag{33}$$

where the parameters θ_1 and μ_1 are defined as

$$\begin{aligned} \theta_1^2 &= \lambda_m^2 + V/2 + \sqrt{V^2/4 + S} \\ \mu_1^2 &= \lambda_m^2 + V/2 - \sqrt{V^2/4 + S}. \end{aligned} \tag{34}$$

Case 2 $V^2/4 + S = 0$

The general solution of Eq. (31) in this case can be expressed as

$$\begin{aligned} f(y) = {} & c_1\cos\text{h}(\lambda_m y) + c_2\sin\text{h}(\lambda_m y) + c_3\cos\text{h}(\theta_2 y) + c_4\sin\text{h}(\theta_2 y) \\ & + y\left(c_5\cos\text{h}(\theta_2 y) + c_6\sin\text{h}(\theta_2 y)\right) \end{aligned} \tag{35}$$

where $\theta_2^2 = \lambda_m^2 + V/2$.

Case 3 $V^2/4 + S < 0$

The general solutions of Eq. (31) in this case may be written as

$$\begin{aligned} f(y) = {} & c_1 \cos\,\mathrm{h}\,(\lambda_m y) + c_2 \sin\,\mathrm{h}\,(\lambda_m y) + c_3 \cos\,\mathrm{h}\,(\theta_3 y)\cos\,(\mu_3 y) \\ & + c_4 \cos\,\mathrm{h}\,(\theta_3 y)\sin\,(\mu_3 y) + c_5 \sin\,\mathrm{h}\,(\theta_3 y)\cos\,(\mu_3 y) + c_6 \sin\,\mathrm{h}\,(\theta_3 y)\sin\,(\mu_3 y) \end{aligned} \tag{36}$$

where

$$\begin{aligned} \theta_3^2 &= \frac{1}{2}\left(\sqrt{\lambda_m^4 + V\lambda_m^2 - S} + \lambda_m^2 + V/2\right) \\ \mu_3^2 &= \frac{1}{2}\left(\sqrt{\lambda_m^4 + V\lambda_m^2 - S} - \lambda_m^2 - V/2\right) \end{aligned} \tag{37}$$

To solve Eq. (24a), substituting the proposed series solution (30b) into Eq. (24a) yields an ordinary differential equation, which its general solution is given by

$$g(y) = c_7 \sin\,\mathrm{h}(\zeta y) + c_8 \cos\,\mathrm{h}(\zeta y) \tag{38}$$

where

$$\zeta = \sqrt{\lambda_m^2 + \hat{A}/\hat{B}} \tag{39}$$

Upon substitution Eq. (30) into Eq. (26), the general solution for the rotation functions can be obtained.

3.4 Thermal loading conditions

In this section, to investigate the effect of assumption type of temperature distribution through the thickness on thermal buckling behavior of FG plate, three types of thermal loading as uniform temperature raise, nonlinear and linear temperature distribution across the plate thickness are considered.

3.4.1 Uniform temperature raise (UTR)

It is assumed that the initial uniform temperature of the FG plate is T_i, and the temperature is uniformly raised to a final value T_f such that the plate buckles. The temperature change is $\Delta T = T_f - T_i$, and the thermal force resultant can be obtained by using Eq. (10b) as

$$N^T = h\Delta T\left(\alpha_m E_m + \frac{\alpha_m E_{cm} + \alpha_{cm} E_m}{n+1} + \frac{\alpha_{cm} E_{cm}}{2n+1}\right)/(1-\nu). \tag{40}$$

3.4.2 Nonlinear temperature distribution through the thickness (NTD)

The temperature field assumed to be uniform over the plate surface but varying along the thickness direction due to heat conduction. In such a case, the temperature distribution along the thickness can be obtained by solving the steady-state heat transfer equation as

$$\frac{d}{dz}\left(K(z)\frac{dT(z)}{dz}\right) = 0 \tag{41}$$

with the boundary conditions $T(h/2) = T_c$ and $T(-h/2) = T_m$, where T_c and T_m are the temperatures of full-ceramic and full-metallic surfaces, respectively. The coefficient of thermal conductivity $K(z)$ is assumed to obey the power-law relation (1). Substituting Eq. (1) into Eq. (41) yields a second-order differential equation in terms of temperature which can be written as

$$-\frac{d^2T}{dr^2} + \frac{nK_{cm}r^{n-1}}{K_m + K_{cm}r^n}\frac{dT}{dr} = 0 \tag{42}$$

where

$$r = \frac{1}{2} + \frac{z}{h}. \tag{43}$$

The differential Eq. (42) can be easily solved by using the polynomial series. Thus, the temperature distribution across the plate thickness is obtained as

$$T(z) = T_m + r\Delta T \frac{\sum_{k=0}^{\infty}\left(\frac{1}{nk+1}\left(\frac{-K_{cm}r^n}{K_m}\right)^k\right)}{\sum_{k=0}^{\infty}\left(\frac{1}{nk+1}\left(\frac{-K_{cm}}{K_m}\right)^k\right)}, \qquad \Delta T = T_c - T_m \tag{44}$$

Substitution of Eq. (44) into Eq. (10b) yields the thermal force resultant as

$$N^T = \left(T_m h\left(\alpha_m E_m + \frac{\alpha_m E_{cm} + \alpha_{cm} E_m}{n+1} + \frac{\alpha_{cm} E_{cm}}{2n+1}\right) + h\Delta T \frac{X_1}{X_2}\right)/(1-\nu) \tag{45}$$

where

$$\begin{aligned} X_1 &= \sum_{k=0}^{\infty}\left(\frac{1}{nk+1}\left(\frac{-K_{cm}}{K_m}\right)^k\left(\frac{\alpha_m E_m}{nk+2} + \frac{\alpha_m E_{cm} + \alpha_{cm} E_m}{n(k+1)+2} + \frac{\alpha_{cm} E_{cm}}{n(k+2)+2}\right)\right) \\ X_2 &= \sum_{k=0}^{\infty}\left(\frac{1}{nk+1}\left(\frac{-K_{cm}}{K_m}\right)^k\right). \end{aligned} \tag{46}$$

3.4.3 Linear temperature distribution through the thickness (LTD)

As an approximation, consider the following linear temperature distribution along the thickness coordinate of the FG plate as

$$T(z) = \frac{\Delta T}{h}\left(z + \frac{h}{2}\right) + T_m, \quad \Delta T = T_c - T_m \tag{47}$$

where variable z is measured from the middle plane of the plate. It should be noted that for homogeneous isotropic plates ($n = 0$), the linear temperature distribution (47) is exactly justified.
The thermal force resultant can be expressed by using Eq. (10b) as

$$\begin{aligned} N^T = \Bigg(&h\Delta T\left(\frac{\alpha_m E_m}{2} + \frac{\alpha_m E_{cm} + \alpha_{cm} E_m}{n+2} + \frac{\alpha_{cm} E_{cm}}{2n+2}\right) \\ &+ hT_m\left(\alpha_m E_m + \frac{\alpha_m E_{cm} + \alpha_{cm} E_m}{n+1} + \frac{\alpha_{cm} E_{cm}}{2n+1}\right)\Bigg)/(1-\nu). \end{aligned} \tag{48}$$

3.5 Critical buckling temperature difference

To investigate thermoelastic buckling behavior of FG plate with definite material properties and geometric parameters, the boundary conditions at the two other edges of the rectangular plate in x direction (i.e. $y = 0$ and $y = b$) should be also specified. The FG plate may be under different combination of classical boundary conditions, including clamped, hard simply supported and free in x direction. It should be noted that the boundary conditions of the plate are assumed to be movable in the plane of the plate (i.e. $u \neq 0, v \neq 0$), whereas there are no middle-surface force resultants (i.e. $N^1_{xx} = N^1_{yy} = N^1_{xy} = 0$) [18,23]. These boundary conditions that are developed from the principle of minimum total potential energy together with application of the adjacent equilibrium criterion are as follows:

$$\begin{aligned} &\text{For clamped edges:} && w^1 = w^1_{,y} = \psi^1_x = \psi^1_y = 0 \\ &\text{For simply supported (hard type) edges:} && w^1 = \psi^1_x = M^1_{yy} = P^1_{yy} = 0 \\ &\text{For free edges:} && M^1_{yy} = P^1_{yy} = M^1_{xy} - \eta P^1_{xy} = \left(Q^1_y - \beta R^1_y\right) + \eta\left(2P^1_{xy,x} + P^1_{yy,y}\right) - N^T w^1_{,y} = 0. \end{aligned} \tag{49}$$

Table 1 Comparison of the critical buckling temperature difference for a simply supported functionally graded plate subjected to different thermal loads ($a/b = 1$)

Temperature distribution	n		$b/h = 10$	$b/h = 20$	$b/h = 40$	$b/h = 60$	$b/h = 80$	$b/h = 100$
UTR	0	Ref. [6]	1617.484	421.516	106.492	47.424	26.693	17.088
		Present	1617.4842	421.5163	106.4917	47.4236	26.6929	17.0880
	1	Ref. [6]	757.891	196.257	49.500	22.037	12.402	7.939
		Present	757.8906	196.2568	49.5003	22.0370	12.4022	7.9391
	5	Ref. [6]	678.926	178.528	45.213	20.144	11.340	7.260
		Present	678.9260	178.5284	45.2133	20.1436	11.3396	7.2599
	10	Ref. [6]	692.519	183.141	46.455	20.703	11.657	7.462
		Present	692.5191	183.1407	46.4548	20.7030	11.6566	7.4618
LTD	0	Ref. [6]	3224.968	833.032	202.984	84.848	43.387	24.177
		Present	3224.9684	833.0325	202.9844	84.8480	43.3871	24.1773
	1	Ref. [6]	1412.023	358.696	83.459	31.952	13.882	5.513
		Present	1412.0227	358.6958	83.4590	31.9523	13.8825	5.5133
	5	Ref. [6]	1160.024	298.693	69.219	26.067	10.913	3.891
		Present	1160.0245	298.693	69.2191	26.0666	10.9126	3.8907
	10	Ref. [6]	1218.328	315.677	73.461	27.826	11.797	4.364
		Present	1218.3281	315.6770	73.4614	27.8263	11.7969	4.3636
NTD	0	Ref. [6]	3224.968	833.032	202.984	84.848	43.387	24.177
		Present	3224.9683	833.0322	202.9841	84.8484	43.3872	24.1770
	1	Ref. [6]	1960.018	497.903	115.849	44.352	19.270	7.652
		Present	1960.0184	497.9032	115.8492	44.3521	19.2700	7.6518
	5	Ref. [6]	1450.769	373.557	86.568	32.600	13.648	4.866
		Present	1450.7690	373.5571	86.5684	32.6003	13.6479	4.8656
	10	Ref. [6]	1408.132	364.857	84.904	32.162	13.634	5.044
		Present	1408.1318	364.8566	84.9038	32.1617	13.6336	5.0439

There are unknown parameters including constant coefficients c_i, $(i = 1.8)$, temperature difference (ΔT) and the number of half-waves in the x direction (m) in general solutions for transverse displacement and boundary layer function. By imposing the boundary conditions at two edges of the rectangular plate in x direction ($y = 0$ and $y = b$), a set of homogenous algebraic equations is obtained in terms of c_i, $(i = 1.8)$ and ΔT for each longitudinal half-wave number (m). To obtain a nontrivial solution of the system, the determinant of the eighth-order coefficient matrix is set equal to zero for ΔT, which results in the characteristic equation. Solving this equation, the buckling temperature differences of the FG plate are calculated. The lowest value among all these ΔT's for each m is known as the critical buckling temperature difference (ΔT_{cr}).

For simplicity and convenience, the letters F, S and C are used to denote a free edge, a simply supported edge (hard type) and a clamped edge, respectively.

4 Validation of the results

In order to validate the accuracy of the present formulations, a comparison has been carried out with the results obtained by Javaheri and Eslami [6] based on the HSDT, for all edges simply supported FG plates. The critical buckling temperature difference has been listed in Table 1 for a square simply supported plate subjected to different temperature distribution across the thickness and side-thickness ratios. As this table shows, the present results have an excellent agreement with those reported in Ref. [6].

5 Results and discussion

After verifying the accuracy of the present solution, in order to obtain the following new results, it is assumed that the functionally graded plate is made of a mixture of aluminum and alumina. The Young modulus, coefficient of thermal expansion and thermal conductivity for aluminum are $E_m = 70\,\text{GPa}$, $\alpha_m = 23 \times 10^{-6}/^{\circ}\text{C}$, $K_m = 204\,\text{W/m}^{\circ}\text{K}$ and for alumina are $E_c = 380\,\text{GPa}$, $\alpha_c = 7.4 \times 10^{-6}/^{\circ}\text{C}$, $K_c = 10.4\,\text{W/m}^{\circ}\text{K}$, respectively. The temperature in the full-metal surface of the plate is assumed to be 5°C. Also, the Poisson's ratio of the plate is assumed to be constant through the thickness and equal to 0.3. In order to study the temperature distribution along the thickness of the functionally graded plate based on the Eq. (44), the nondimensional temperature change $((T(z) - T_m)/(T_c - T_m))$ along the thickness for different values of power of

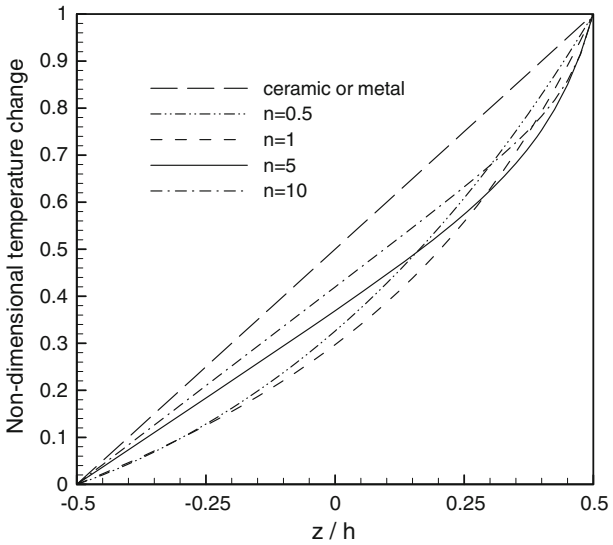

Fig. 1 Non-dimensional temperature change across the thickness for different values of power of FGM

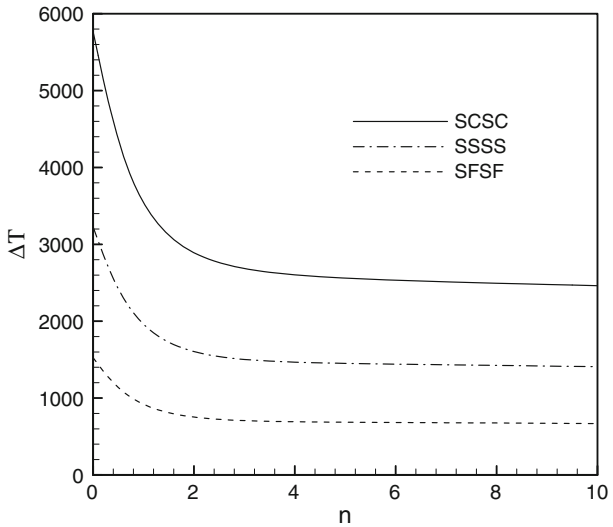

Fig. 2 The critical buckling temperature difference for a FG plate with symmetric boundary conditions versus the power of FGM ($a/b = 1$, $h/b = 0.1$)

FGM is presented in Fig. 1. It can be seen from this figure that the temperature change along the thickness in a homogeneous plate made of full-metal or full-ceramic is linear, whereas for a functionally graded plate it is nonlinear, as expected. It can also be seen that the temperature at any internal point through the thickness of the plate made of an isotropic material is always higher than those of FG plates, which is an important property of FG plates. In Fig. 2, the critical buckling temperature difference for a FG plate with symmetric boundary conditions is plotted versus the power of FGM, under nonlinear temperature distribution across the thickness. This figure shows that the critical buckling temperature difference decreases significantly with increasing the power of FGM. This is due to the fact that increasing the power of FGM increases the volume fraction of metal. Also, the variation of critical buckling temperature for the power of FGM more than 2 is small.

In Fig. 3, the critical buckling temperature difference versus the aspect ratio (a/b) is depicted for a $SCSC$ plate under nonlinear temperature distribution across the thickness. It can be observed that the critical thermal buckling mode may change as the aspect ratio increases. The effect of the aspect ratio for different kinds of thermal loads on the critical buckling temperature difference is presented in Fig. 4. The FG plate is assumed to have clamped edges in x direction. It can be found that the critical buckling temperature difference generally

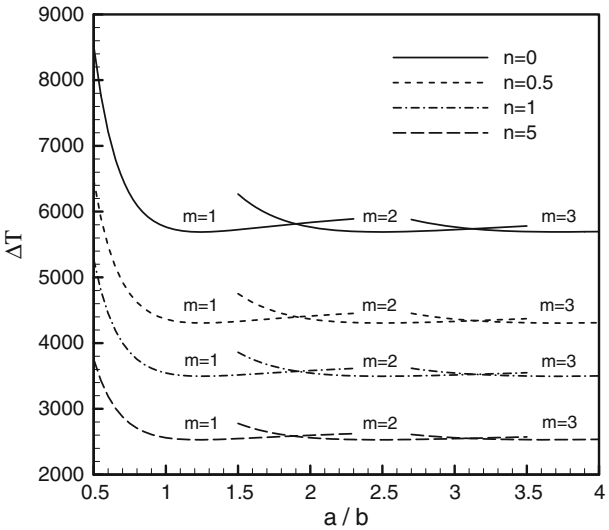

Fig. 3 The critical buckling temperature difference a $SCSC$ plate versus the aspect ratio ($h/b = 0.1$)

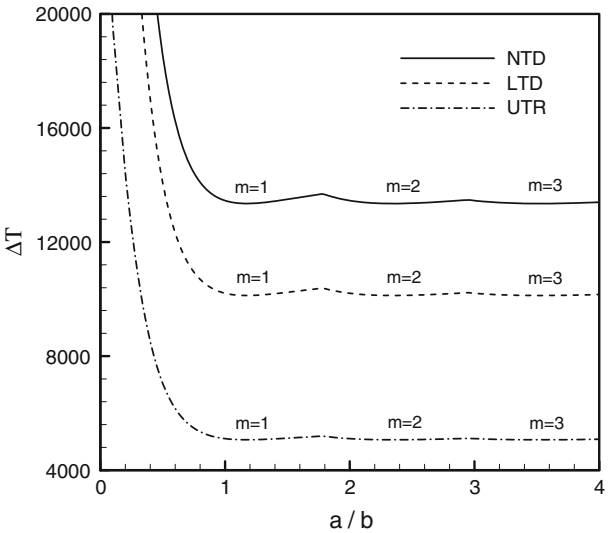

Fig. 4 Effect of the aspect ratio for different kinds of thermal loads on the critical buckling temperature difference of a $SCSC$ plate ($h/b = 0.2$, $n = 0.5$)

decreases by increasing the aspect ratio. Also, the critical buckling temperature difference of the FG plate under linear temperature distribution across the thickness is greater than the one under uniform temperature raise and less than the one under nonlinear temperature distribution across the thickness. Moreover, the effect of the temperature distribution along the thickness on the critical buckling temperature of a $SCSF$ plate with different power of FGM is investigated in Fig. 5. It can be seen that the critical buckling temperature difference of the fully ceramic plate ($n = 0$) under linear and nonlinear temperature distribution across the thickness is identical, also, for $0 < n \leq 10$, by increasing the power of FGM, the difference between them increases first, and then reduced. It should be noted that both curves in infinite value of power of FGM joined to each other.

The critical buckling temperature difference versus the thickness-side ratio (h/b) for a $SSSC$ plate under nonlinear temperature distribution with different values of power of FGM is demonstrated in Fig. 6. It is observed that increasing the thickness of the FG plate severely increases the critical buckling temperature difference. Such behavior is due to the influence of the transverse shear deformation in the plate. Also, it can be concluded that in a specific thickness-side ratio, the critical buckling temperature of the FG plates is between those of full-ceramic and full-metallic plates.

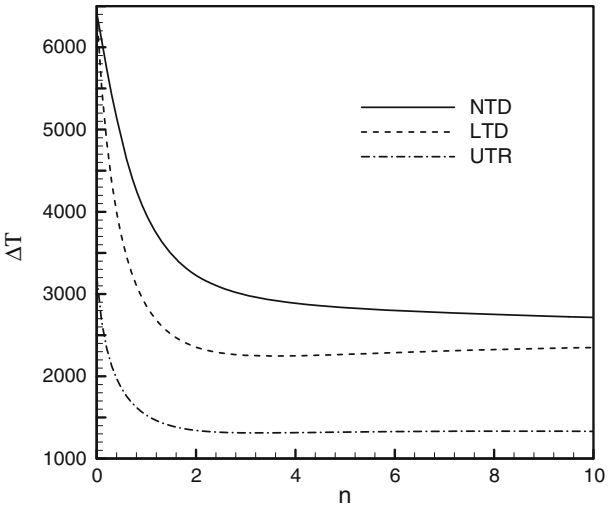

Fig. 5 Effect of the various temperature distributions across the thickness on the critical buckling temperature of a $SCSF$ plate with different values of power of FGM ($a/b = 1,\ h/b = 0.2$)

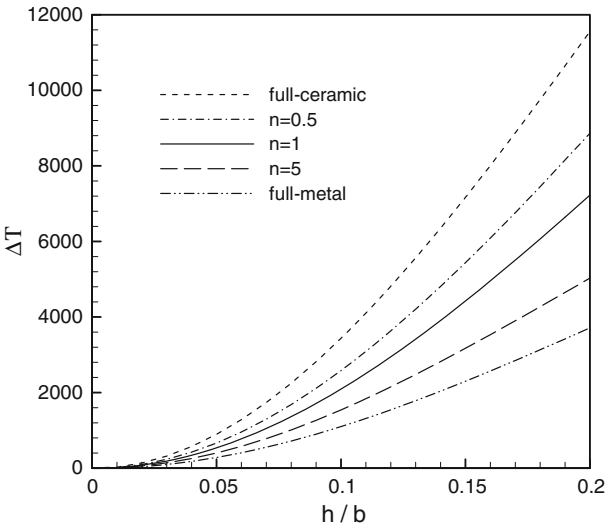

Fig. 6 The critical buckling temperature difference versus the thickness-side ratio for a $SSSC$ plate with different values of power of FGM ($a/b = 2$)

The critical buckling temperature difference has been tabulated in Table 2 for a plate under the nonlinear temperature distribution across the thickness. The results are obtained for different boundary conditions, some powers of FGM and various thickness-side and aspect ratios. From the presented results in this table, it is observed that the lowest and highest values of ΔT_{cr} correspond to $SFSF$ and $SCSC$ cases, respectively. Thus, more constraints at the edges increase the stiffness of the FG plate, resulting in a higher critical buckling temperature difference.

6 Conclusions

In this research work, thermal buckling analysis of thick functionally graded rectangular plates in thermal environment has been presented. Based on the higher-order shear deformation theory of Reddy, the equilibrium and stability equations of thick functionally graded rectangular plates have been derived. The governing stability equations of FG rectangular plates have been decoupled and converted into two independent equations. The Levy-type solution has been employed for solving the decoupled equations of FG rectangular plates with two

Table 2 The critical buckling temperature difference for a functionally graded rectangular plate under the nonlinear temperature distribution across the thickness with different boundary conditions

n	$\frac{a}{b}$	$\frac{h}{b}$	$SCSC$	$SCSS$	$SSSS$	$SCSF$	$SSSF$	$SFSF$
0	0.5	0.1	8521.3697	7909.7263	7484.4781	5924.6887	5896.7679	5736.4811
		0.2	23637.2875	22651.4296	21903.9401	17760.5702	17730.4976	17489.0799
	1	0.1	5766.0064	4182.4515	3224.9683	1810.1862	1692.4485	1525.2149
		0.2	17286.7105	13631.3760	11156.3660	6419.4427	6097.5808	5633.7000
	1.5	0.1	5725.2270	3600.5391	2363.2470	1008.0910	810.7364	678.4565
		0.2	17361.4980	12011.1585	8487.4493	3713.7582	3056.2261	2636.6941
1	0.5	0.1	5275.1281	4881.0037	4609.1889	3644.8873	3626.3014	3522.9330
		0.2	15258.7942	14559.1299	14035.0852	14608.7787	11296.7094	11121.1978
	1	0.1	3545.2805	2554.0664	1960.0184	1096.7728	1023.6397	920.0159
		0.2	11020.4147	8569.6136	6941.3597	3966.6834	3758.1784	3457.4089
	1.5	0.1	3516.0071	2194.1775	1431.0571	606.4514	485.5827	404.2818
		0.2	11053.3181	7520.4816	5241.7242	2276.2676	1865.1082	1600.2321
5	0.5	0.1	3755.8645	3500.2302	3320.5477	2630.6044	2619.4340	2552.5204
		0.2	9881.3288	9516.7820	9236.4616	9484.1409	7534.7221	7449.1792
	1	0.1	2561.1926	1872.1889	1450.7690	812.0894	760.2201	686.3085
		0.2	7340.7476	5891.1043	4885.6172	2835.2156	2701.2897	2509.1185
	1.5	0.1	2547.0719	1614.5732	1064.7964	450.8696	362.1954	303.0442
		0.2	7382.1869	5217.1595	3752.2650	1653.5220	1366.4599	1185.8967
10	0.5	0.1	3591.4901	3355.5724	3188.6031	2528.4376	2518.4105	2456.7231
		0.2	9144.7795	8833.2811	8591.5901	8786.2878	7042.0952	6971.4095
	1	0.1	2462.2704	1809.8277	1408.1318	788.6095	739.0705	668.3455
		0.2	6858.5318	5563.1042	4651.5438	2716.1921	2592.7752	2416.5217
	1.5	0.1	245.1141	1563.1276	1035.4629	438.8055	353.0469	296.0129
		0.2	6902.1004	4942.1781	3594.6403	1593.9662	1321.3258	1151.4927

opposite edges simply supported. To certify the accuracy of the present formulations, the results obtained by the present analysis have been compared with their counterparts in the literature for special case of simply supported functionally graded plates. Also, parametric studies have been performed to examine the influences of power of functionally graded material, aspect ratio, thickness-side ratio, thermal loading conditions and different combinations of boundary conditions on the critical buckling temperature of aluminum/alumina functionally graded rectangular plates. The presented formulations and results will be a useful benchmark for researchers to check out their analytical and numerical methods and also for engineering designers deal with analyzing functionally graded plates in thermal environment in the future.

Finally, some general conclusions can be summarized as follows:

1) The temperature at any internal point through the thickness of the plate made of an isotropic material is always higher than those of FG plates. This is an important property of functionally graded materials.
2) The critical buckling temperature difference of FG plates generally decreases by increasing the aspect ratio.
3) In the FG plates, the solution of the steady-state heat transfer equation results in a nonlinear temperature distribution across the thickness of the plate. As this temperature distribution overestimates the critical buckling temperature compared to the assumption of linear temperature distribution and uniform temperature raise.
4) The critical buckling temperature difference of FG plates increases when the thickness-side ratio increases. However, it decreases when the power of FGM increases.
5) For some boundary conditions, by increasing the aspect ratio, the critical thermal buckling mode may be changed.
6) By increasing the edge constraint (from clamped to simply supported to free), the critical buckling temperature difference increases.

Appendix A

In order to obtain the boundary layer Eqs. (24a), (22a) and (22b) are differentiated with respect to y and x, respectively, and finally the obtained results are subtracted. Also, to derive Eq. (24b), differentiating Eq. (22a), (22b) with respect to x and y, respectively, and then adding the result, the following equation can be obtained

$$\hat{C}\nabla^2\varphi_3 - \hat{A}\left(\varphi_3 + \nabla^2 w^1\right) - \hat{H}\nabla^4 w^1 = 0 \tag{A1}$$

Omitting the term $\nabla^2\varphi_3$ from Eqs. (22c) and (A1) leads to

$$\varphi_3 = \frac{\hat{F}\hat{C} - \hat{H}^2}{\hat{A}\left(\hat{C} + \hat{H}\right)}\nabla^4 w^1 - \nabla^2 w^1 - \frac{\hat{C}}{\hat{A}\left(\hat{C} + \hat{H}\right)}\left(N^0_{xx} w^1_{,xx} + 2N^0_{xy} w^1_{,xy} + N^0_{yy} w^1_{,yy}\right) \tag{A2}$$

By substituting Eq. (A2) into Eq. (22c), the interior Eq. (24b) is achieved.

Furthermore, from Eq. (22a), (22b), the rotation functions can be expressed as

$$\psi^1_x = \frac{\hat{C}}{\hat{A}}\varphi_{3,x} + \frac{\hat{B}}{\hat{A}}\varphi_{4,y} - \frac{\hat{H}}{\hat{A}}\nabla^2 w^1_{,x} - w^1_{,x} \tag{A3}$$

$$\psi^1_y = \frac{\hat{C}}{\hat{A}}\varphi_{3,y} - \frac{\hat{B}}{\hat{A}}\varphi_{4,x} - \frac{\hat{H}}{\hat{A}}\nabla^2 w^1_{,y} - w^1_{,y} \tag{A4}$$

Substituting Eq. (A2) into the above equations, Eq. (26) can be obtained.

References

1. Javaheri, R., Eslami, M.R.: Thermal buckling of functionally graded plates. AIAA J. **40**, 162–169 (2002)
2. Samsam Shariat, B.A., Eslami, M.R.: Buckling of functionally graded plates under in-plane compressive loading based on the first order plate theory. In: Proceeding of the Fifth International Conference on Composite Science and Technology. Sharjah, UAE (2005)
3. Wu, L.: Thermal buckling of a simply supported moderately thick rectangular FGM plate. Compos. Struct. **64**, 211–218 (2004)
4. Reddy, J.N.: A simple higher-order theory for laminated composite plates. J. Appl. Mech. **51**, 745–752 (1984)
5. Reddy, J.N.: Analysis of functionally graded materials. Int. J. Numer. Methods Eng. **47**, 663–684 (2000)
6. Javaheri, R., Eslami, M.R.: Thermal buckling of functionally graded plates based on higher order theory. J. Therm. Stress **25**, 603–625 (2002)
7. Ma, L.S., Wang, T.J.: Relationships between axisymmetric bending and buckling solutions of FGM circular plates based on third-order plate theory and classical plate theory. Int. J. Solids Struct. **41**, 85–101 (2004)
8. Najafizadeh, M.M., Heydari, H.R.: Thermal buckling of functionally graded circular plates based on higher order shear deformation plate theory. Eur. J. Mech. A Solids **23**, 1085–1100 (2004)
9. Najafizadeh, M.M., Heydari, H.R.: An exact solution for buckling of functionally graded circular plates based on higher order shear deformation plate theory under uniform radial compression. Int. J. Mech. Sci. **50**, 603–612 (2008)
10. Naghdabadi, R., Hosseini Kordkheili, S.A.: A finite element formulation for analysis of functionally graded plates and shells. Arch. Appl. Mech. **74**, 375–386 (2005)
11. Samsam Shariat, B.A., Eslami, M.R.: Buckling of thick functionally graded plates under mechanical and thermal loads. Compos. Struct. **78**, 433–439 (2007)
12. Saidi, A.R., Rasouli, A., Sahraee, S.: Axisymmetric bending and buckling analysis of thick functionally graded circular plates using unconstrained third-order shear deformation plate theory. Compos. Struct. **89**, 110–119 (2009)
13. Bodaghi, M., Saidi, A.R.: Stability analysis of functionally graded rectangular plates under nonlinearly varying in-plane loading resting on elastic foundation. Arch. Appl. Mech. (2010). doi:10.1007/s00419-010-0449-0
14. Nosier, A., Reddy, J.N.: On boundary layer and interior equations for higher-order theories of plates. Z Angew Math. Mech. **72**(12), 657–666 (1992)
15. Saidi, A.R., Jomehzadeh, E.: On analytical approach for the bending/stretching of linearly elastic functionally graded rectangular plates with two opposite edges simply supported. Proc. I Mech. E Part C J. Mech. Eng. Sci. **223**, 2009–2016 (2009)
16. Mohammadi, M., Saidi, A.R., Jomehzadeh, E.: A novel analytical approach for buckling analysis of moderately thick functionally graded rectangular plates with two opposite edges simply supported. Proc. IMechE Part C J. Mech. Eng. Sci. **224**, 1831–1841 (2010)
17. Praveen, G.N., Reddy, J.N.: Nonlinear transient thermoelastic analysis of functionally graded ceramic-metal plates. Int. J. Solids Struct. **35**, 4457–4476 (1998)
18. Brush, D.O., Almroth, B.O.: Buckling of Bars, Plates, and Shells. McGraw–Hill, New York (1975)
19. Reddy, J.N.: Energy Principles and Variational Methods in Applied Mechanics. John Wiley, New York (1984)
20. Reddy, J.N.: Theory and Analysis of Elastic Plates. Taylor & Francis, Philadelphia (1999)
21. Abrate, S.: Functionally graded plates behave like homogeneous plates. Compos. Part B **39**, 151–158 (2008)
22. Meyers, C.A., Hyer, M.W.: Thermal buckling and postbuckling of symmetrically laminated composite plates. J. Therm. Stress **14**, 519–540 (1991)
23. Amabili, M.: Nonlinear Vibrations and Stability of Shells and Plates. Cambridge University Press, New York (2008)